23rd ABCM International Congress of Mechanical Engineering
December 6-11, 2015, Rio de Janeiro, RJ, Brazil

DIGITAL PROTOTYPING OF A MAGNETORHEOLOGICAL KNEE FOR PROSTHESES AND EXOSKELETONS

Rafhael Milanezi de Andrade
Arnaldo Gomes Leal Junior
Luiz Henrique Dalvi Alves
Antônio Bento Filho
Department of Mechanical Engineering, Universidade Federal do Espirito Santo, Avenida Fernando Ferrari, 514, Goiabeiras, 29075-910, Vitória, ES, Brazil.
rafhael.andrade@ufes.br, arnaldo_lealjunior@hotmail.com, luizhdalvi@hotmail.com, antonio.bento@ufes.br

Marcos Pinotti Barbosa
Department of Mechanical Engineering, Universidade Federal de Minas Gerais, Av. Antônio Carlos, 6627, Pampulha, 31270-901, Belo Horizonte, MG, Brazil.
pinotti@demec.ufmg.br

Abstract.

Magnetorheological (MR) fluids are smart materials which can have their properties controlled by an induced magnetic field. MR fluids have been used in devices with multiple purposes such as damping vibrations in structures and vehicle suspensions, in valves, in prostheses and others. MR actuators are examples of such devices. With MR fluid, the actuator possesses multiple functions working as motor, clutch, or brake. Since the knee develops active torque and brake function in human gait, a MR actuator may be a promising application in order to replace or support the human knee. Despite advances and research in assistive technology, there are no MR actuators being used in such applications yet. The present paper presents the digital prototyping of a MR actuator for knee prostheses and exoskeletons. Digital prototyping is an efficient approach to product development that lets someone design, visualize, and simulate parts and mechatronic devices. It is possible to make detailed design of the device and get the data for dynamic model simulation. The digital prototype's dimensions, mass and inertia properties are used to build the dynamic model for simulations and implementation of a controller. The results show that the developed actuator is promising for the proposed applications, which require multiple functions with compact size and quick response time.

Keywords: *Magnetorheological actuator, prostheses, exoskeletons, digital prototyping, biomechanics.*

1. INTRODUCTION

Magnetorheological fluid (MR) is formed by sols 20% to 40% by volume of magnetizable particles mixed with inert oil, usually mineral based or silicone-based (Rainbow, 1948). When the fluid is subjected to an external magnetic field, particles begin to form columnar structures parallel to the magnetic flux lines. This behavior changes the rheological properties of the fluid, such as viscosity, yield stress and other. The response time is in order of milliseconds (Yang, 2001). Due to these characteristics, MR fluids have been used in dampers, allowing modulate the damping level imposed by the magnetic field, and in power transmission systems that require adjustment of the output torque, as clutches. MR devices are used in various applications in engineering and industry: vehicle suspensions (Sung and Choi, 2008), clutches (Kavlicoglu et al., 2006), brakes (Nguyen and Choi, 2010), structural vibration damping (Takashi and Sano, 2005), intelligent prosthesis ((Carlson et al., 2001) (Dong et al., 2005, 2006)), and others.

In general vehicle suspensions, vibration dampers and intelligent prosthesis can be divided into three main groups: passive, semi-active and active ((Martinez-Villalpando and Herr, 2009) and (Abreu and Ribeiro, 2014)). The passive devices do not allow damping level control and do not require a power source for its operation, they are designed for every application and do not allow performance adjustments (Martinez-Villalpando and Herr, 2009). The semi-active devices only dissipate energy through controllable dampers (Lauwerys et al., 2002). In this case, MR dampers have good efficiency ((Yang, 2001) and (Sung and Choi, 2008)). On the other hand, the active type devices are able to supply and dissipate energy through the actuators and dampers with controllable damping level.

According to Carlson et al., (2001), one of the most interesting applications for MR fluids technology is that of real-time controlled dampers used in advanced prosthetic devices. In such systems, a small magnetorheological damper is used to control the movement of an artificial limb based on inputs from a sensor group. According to the authors, the benefit of an artificial knee with this technology is a more natural gait that automatically adapts to changing speed and terrain. Moreover, according Herr and Wilkenfeld (2003), although semi-active knee prosthesis provides advantages over passive one, it is incapable to producing mechanical energy and therefore cannot replicate the positive work done for certain activities in human knees such as sitting and standing, climbing stairs or ramps and others.

In an attempt to develop prostheses capable to reproduce the human leg movement in these indicated situations, different configurations and devices have been proposed. Martinez-Villalpando and Herr (2009), Garcia et al., (2011) and Filho et al., (2014) propose use of linear serial elastic actuators between the femur and tibia. This configuration presents some characteristics such as tolerance to impact, low mechanical output impedance and passive mechanical energy storage. However, they are heavy devices with high power consumption, making it difficult to use in prosthetics and exoskeletons. Chen and Liao (2010) and Guo and Liao (2012) develop rotating magnetorheological actuators that can work as motor, when need to produce power, as a clutch when necessary to control the output torque, and as brake or damper when it is necessary to dissipate energy. However they have some weak points. In Chen and Liao (2010) the set engine, gearbox and actuator is too big and too heavy to be used in a prosthesis or exoskeleton. In Guo and Liao (2012), despite the appropriate dimensions, the output torque is insufficient for these applications. The device reaches 0.27 Nm at 1300 rpm (36.8 W), but, according Kawamoto e Sankai (2002) and Kapti and Yucenur (2006), the minimum torque required for a normal walk is $T_{min} > 20.0$ Nm. In many cases the required output power is about 100 W or 150 W.

As aforementioned, it is noted that, despite advances and research in the area, it is still necessary to develop specific actuators for many applications. In this paper is developed the digital prototype of a compact, lightweight magnetorheological actuator for use in rotary joints exoskeletons of knees and prostheses. In digital prototyping design is presented the specification of the engine and gearbox assembly and the design of the magnetorheological brake. Moreover are shown the magnetic flux simulation and the 3D prototype. The digital prototype dimensions, mass and inertia properties are used to build the dynamic model for simulations and implementation of a controller.

2. DIGITAL PROTOTYPING DESIGN

Over the years, digital prototyping has been successfully applied in engineering and manufacturing allowing virtually explore a complete product before it's built ((Soyguder and Alli, 2007), and (Wang, 2011)). As reported by Johansson et al. (2004), the digital prototyping has been important to development of industrial robots, reducing the time robot programming phase. According to the authors, the robot task can be simulated in a virtual model of the work cell when still only a digital prototype of the workpiece exists and the risk of technical failure for a transition can be reduced. In this way, before manufacture of the proposed serial elastic actuator, is presented in this paper its digital prototyping.

2.1 Model

The aim of the design is to develop an actuator for knee prostheses and exoskeletons able to provide both active and passive torque according to the task. In situations where braking is needed (passive torque), a magnetorheological brake provides the necessary torque between outer (connect to upper limb) and inner parts (connect to lower leg), by controlling the current applied to the coil. When active torque is needed, a Maxon DC Motor (EC 60 flat Ø68 mm, brushless, 100 Watt) with a Harmonic Drive CSD-17-2UH, 1:100 provides torque up to 65 Nm, enough for a person to climb ramps and stairs (Riener et al., 2002).

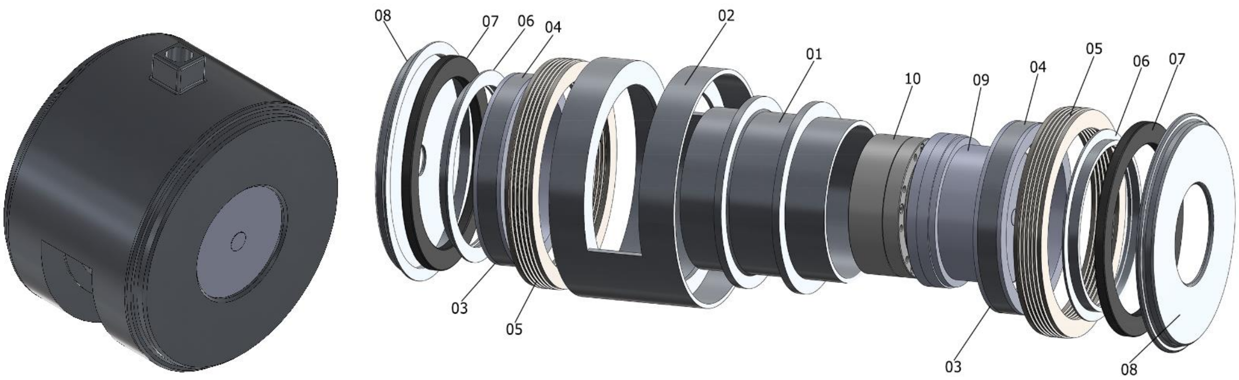

(a) (b)

Figure 1. Actuator's 3D view. (a) Final assembly of the actuator. (b) Exploded view

Figure 1 shows the actuator's 3D view. In order to produce the necessary active torque, a DC motor (09) and a Harmonic drive (10) are located into the core of the system, the output of this unit is connected to the outer housing of the actuator (02) made of aluminum and connected to the upper leg. An aluminum cylindrical piece (01) is the inner piece of the actuator. This part is connected to the lower limb and houses both motor and drive inside it. On its outside, there are two sets of coils consisting of a cobalt-iron alloy core (03), a copper winding and an aluminum cover (04). The sets also work as a platform for the inner steel disks (05). The outer discs are engaged in the outer housing (02). MR fluids are filled between the outer and inner disks and are used in shear mode to produce torque. The chosen fluid is the MRF-132DG provided by LORD corporation. A pair of thin section bearings (07) is used in order to connect and allow relative motion between inner and outer part. Aluminum side plates (08) will be attached to the outer housing, covering the sides of the actuator.

All the design process is made thinking of a way to combine magnetic and mechanical requirements of the actuator and feasibility of the manufacturing. Overall height of the actuator is 106 mm and its width is 72 mm, final weight is expected to be circa 2 kg.

2.2 Brake design

In order to compute the torque generated by the brake part of the actuator, the following equation is used:

$$T = \int_{ri}^{ro} \tau_{MR} r_D dA \quad (1)$$

Where τ_{MR} is the shear stress of the fluid, r_D is the radius of the disks and A is the effective surface area of the disks. The surface area can be described in terms of the number of working gaps (N_g), and the radii of the inner and outer disks. Then, the torque equation can then be rewritten as:

$$T = 2N\pi\int_{ri}^{ro}(\tau_Y + \eta\dot{\gamma})r_D(r_D dr_D) = 2N_g\pi\left[\frac{\tau_Y}{3}\left(r_o^{\,3} - r_i^{\,3}\right) + \frac{\omega\eta}{4g_D}\left(r_o^{\,4} - r_i^{\,4}\right)\right] \quad (2)$$

Where τ_Y is the yield stress related to the applied magnetic flux density obtained by consulting the MR fluid datasheet provided by the manufacturer, η is the off-field viscosity and $\dot{\gamma}$ is the shear rate written as a function of the radius, the length of the working gap (g_D) and the angular velocity (ω).

The dimensions are set as *ri*=43 mm and *ro*=51 mm. The number of gaps is *N*=20 and the length of each gap is g_D =0.5 mm. The shear stress value is set as 25 kPa. Fluid properties are provided by the manufacturer. The accounted value for the torque produced by the actuator is about 111 Nm. It was shown that the minimum resistive torque necessary for the human walk is about 20 Nm and the peak resistive torque of activities such as down stairs can reach up to 100 Nm (Riener et al., 2002).

In order to assure the correct operation of the actuator, it is important to determine the size of the coil which ensures the specified magnetic field on the fluid area. The coil is a multilayer type with AWG 30 copper wires on cobalt-iron alloy core.

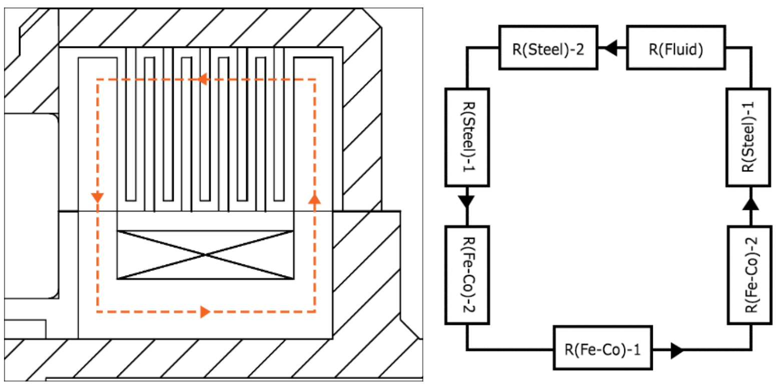

(a) (b)

Figure 2. (a) Magnetic flux path. (b) Magnetic circuit

A magnetic circuit is designed according to the expected loop created once a current is applied. The path is shown on Figure 2 (a). The reluctances circuit is shown on Figure 2 (b). Since the components of the circuit are connected in series, it is possible to assume that the magnetic flux is uniform, and with the magnetic flux density on the fluid area as a design parameter, the flux of the circuit can be expressed as

$$\phi = \pi\left(r_o^{\,2} - r_i^{\,2}\right)B \tag{3}$$

The number of turns for the coil is then calculated as

$$NI = \phi \sum R_i \tag{4}$$

Where N is the number of coils, ϕ is the magnetic flux, I is the input current and R_i is the reluctance of each part. Using a 1.5 A current, the estimated number of turns for the actuator is 365. It's important to point that all this procedures are valid only if no element on the circuit reaches saturation magnetic flux.

A FEM simulation is realized to validate the previous calculations. Using ANSYS workbench, a 2D axisymmetric model is created in order to represent the coil and the other parts relevant to the magnetic circuit. Since the circuit is in series, elements order can be adjusted without compromising the final result. For this simulation the disks and the fluid gap areas are re arranged to simplify the analysis. This methodology is used by other authors before fabrication of MR devices (Grunwald and Olabi, 2008), (Chen and Liao, 2010) and (Guo and Liao 2012)).

B-H curves are used to assign the magnetic properties of 1020 Steel, Cobalt-Iron and MR fluid. Both coil area and aluminum area will receive a magnetic permeability of 1 due to the non-magnetic properties. The input is made in form of current density; the magnetic flux contour and the density are shown in Figure 3.

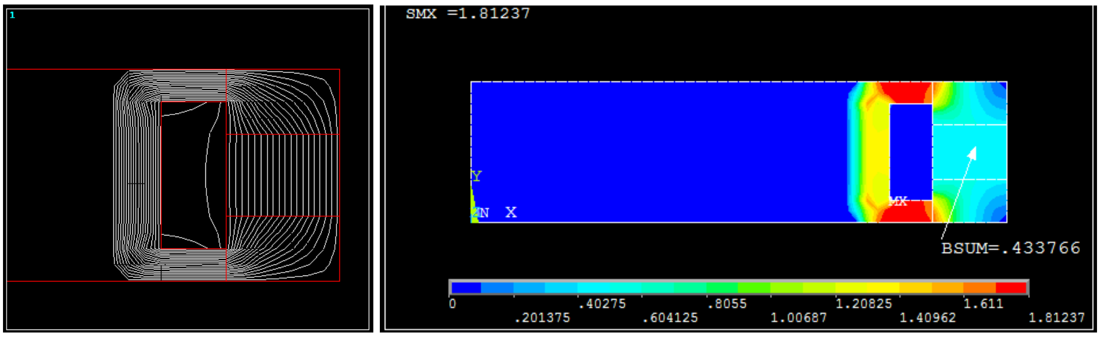

(a) (b)

Figure 3. (a) Magnetic flux contour. (b) Magnetic flux density

The contour result shows the flux lines are distributed as expected, being them normal to the fluid area. The maximum flux density is 1.812 T on the core, the Cobalt-Iron saturation density is 2.2 T, so no saturation occurs. The density calculated on the fluid area is about 0.4337 T which satisfy the project's design requirements.

3. ACTUATOR'S DYNAMIC MODEL

The dynamic model of the actuator, presented in Figure 4, was constructed from the digital prototype data to run a simulation in order to verify its dynamic behavior, bandwidth and validate the project settings. The actuator dynamic model equations are described for closed loop position control. For model simplicity all the connections are rigid. Therefore K1 and K2 are very high numbers and C2 is negligible. The DC motor model is presented as in the literature. Several assumptions are made in this model which the most important are negligible viscous friction and backlash.

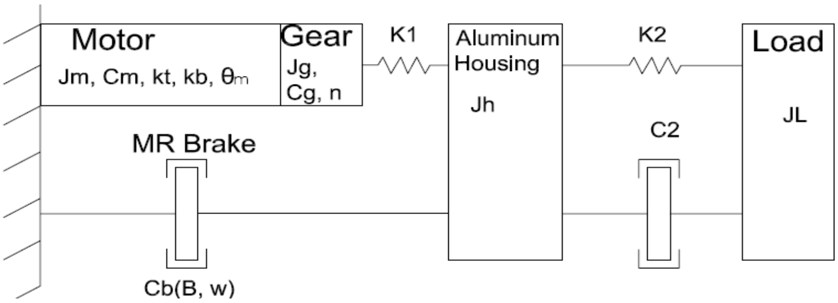

Figure 4. Actuator's dynamic model

Equation (5) describes the electric circuit of the DC motor armature. It contains the inductance (L_a), resistance (R_a), current (i_a), voltage (V_a), back electromotive force constant (k_b) and the angular velocity (ω).

$$L_a \frac{di_a}{dt} + R_a i_a + k_b \omega = V_a \tag{5}$$

Equation (6) represents the mechanical part of the motor which has the system damping ratio (C_e), angular velocity (ω), system inertia (J_T), torque constant (k_T) and armature current (i_a).

$$J_e \frac{d\omega}{dt} + C_e \omega = k_b i_a \tag{6}$$

Where J_e is calculated as in Eq. (7):

$$J_e = J_m + J_G + n^2 (J_L + J_h) \tag{7}$$

The motor inertia in Eq. (7) is the term J_m, J_G is the gear reduction inertia, n is the gear reduction ratio, J_L is the load inertia and J_h is the aluminum housing inertia.

The resistive torque when no magnetic field is applied on the fluid is the second term of Eq. (2), called off-state torque (Gudmundsson et al., 2010). This effect changes the system's damping ratio. The system's damping ratio C_e is defined as in Eq. (8).

$$C_e = C_m + C_G + n^2 C_b = C_m + C_G + n^2 \frac{N_g \pi \eta}{2 g_D} \left(r_o^{\,4} - r_i^{\,4} \right) \tag{8}$$

Where C_m is the motor damping ratio, C_g is the gear reduction inertia, n is the gear reduction ratio, C_b is the damping ratio caused by the torque off-state, indicated in Eq. (8).

Actuator's model second part is the MR brake. The brake consists in a coil to generate the magnetic field and the disks configuration as seen in previous section. Eq. (8) represents the coil model.

$$H = \frac{Ni}{L} \tag{9}$$

In this equation H is the magnetic field force, N is the coil number of turns and L is the coil wire length.

The relation between the magnetic field and the yield stress is obtained by approximation on the experimental curve presented in the MR fluid catalogue. Two independent controllers are employed in this model. There is an integral controller on the MR brake part and a PID controller in the DC motor with gear reduction part. Figure 5 presents the block diagram of the actuator which contains all the methodology and equations discussed above.

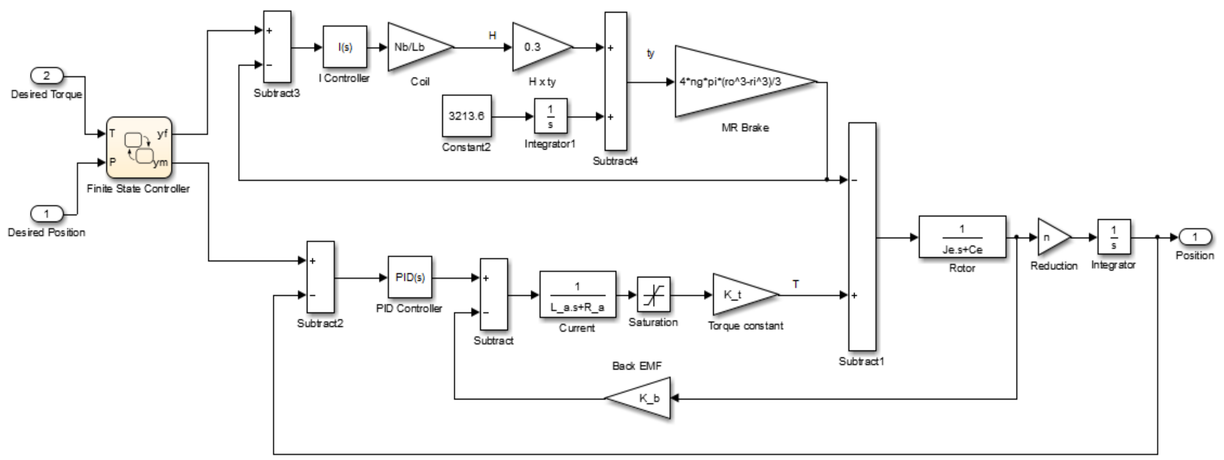

Figure 5. Closed loop transfer function block diagram

The system has two entries. The closed loop first entry is the desired torque on the brake and the second is the desired position on the motor part. Both brake and motor operates independently and there is no simultaneous operation. Motor and brake activation are controlled through a finite state controlled presented in Fig.5. The controller is a logical switch between the brake and motor. It receives torque and position input signals to generate the output signal to motor and brake. Saturation is placed after the current to limit the maximum output current. The current is limited to half of the starting current stated by the catalogue. This limitation prevents the DC motor overheat.

4. RESULTS AND DISCUSSION

The parameters of the actuator dynamic model are obtained by the digital prototype and catalogues of DC motor, gear reduction and MR fluid. Table 1 presents the parameters of all equations described in previous section. These parameters are important to determine the behavior of the system. Moreover these parameters are essential for the controllers tuning.

Table 1. Actuator's parameters

Parameter	Value	Parameter	Value
Armature inductance (La)	1.880E-04 H	Load inertia (J_L)	7.5E-02 Kgm^2
Armature resistance (Ra)	0.307 Ω	Coil wire length (L)	0.015 m
Back-EMF constant (Kb)	5.335E-02 V/s rad	Coil number of turns (N)	365
Torque proportional constant (Kt)	53.4E-03 Nm/A	MR brake inner radius (r_i)	43E-03 m
Gear reduction ratio (n)	0.01	MR brake outer radius (r_o)	51E-03 m
DC motor inertia (J_m)	1.21E-04 Kgm^2	Gaps number (N_g)	20
DC motor damping coefficient (C_m)	9.308E-03 Kgm^2/s	Gap length (g)	0.5E-03 m
Gear reduction inertia (J_G)	3.3E-06 Kgm^2	MR fluid viscosity (η_{MR})	0.112 Pa-s

The controllers are tuned by applying pre-programmed Matlab routines and the controller constants are obtained by an interactive process which began with the well-known Ziegler-Nichols Method. The goal is to obtain a robust controller with a large frequency band.

Table 2 shows the control parameters obtained applying the same methodology and criteria for both controllers. Time response of the system is shown in Figure 6.

Table 2. Controller parameters

Parameters	Kp	Ki	Kd
Integral controller	0	0.51	0
PID controller	3410.82	7705.36	15.22

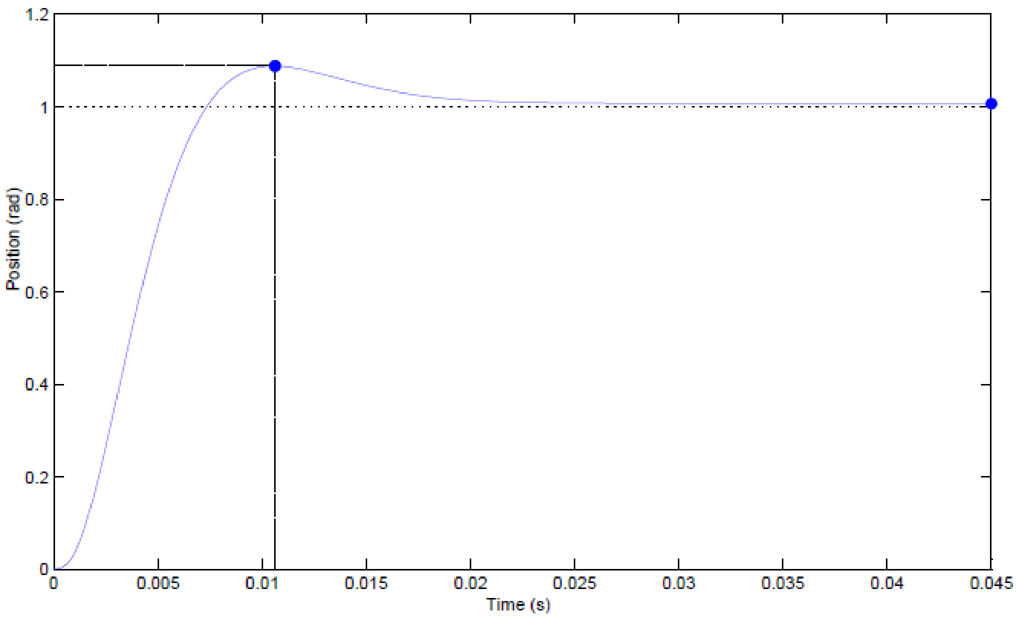

Figure 6. Time response of the system

Figure 6 shows the time response for 1 rad desired position. The analysis displays a 9.3% overshoot and 0.02s settling time. The overshoot below 10% is acceptable for almost all applications and it is coherent with others works ((Guo and Liao, 2012) and (Chen and Liao, 2010)).

Figure 7 indicates a 60 Hz frequency band which is a large band and makes the actuator suitable for any application. On the other hand, the phase margin is 90^o which is very large and undesirable for many applications. But a large phase margin happens with all compliant actuators (Robinson, 2000) and these actuators are employed in many applications, including prostheses and exoskeletons which is the main focus of this work.

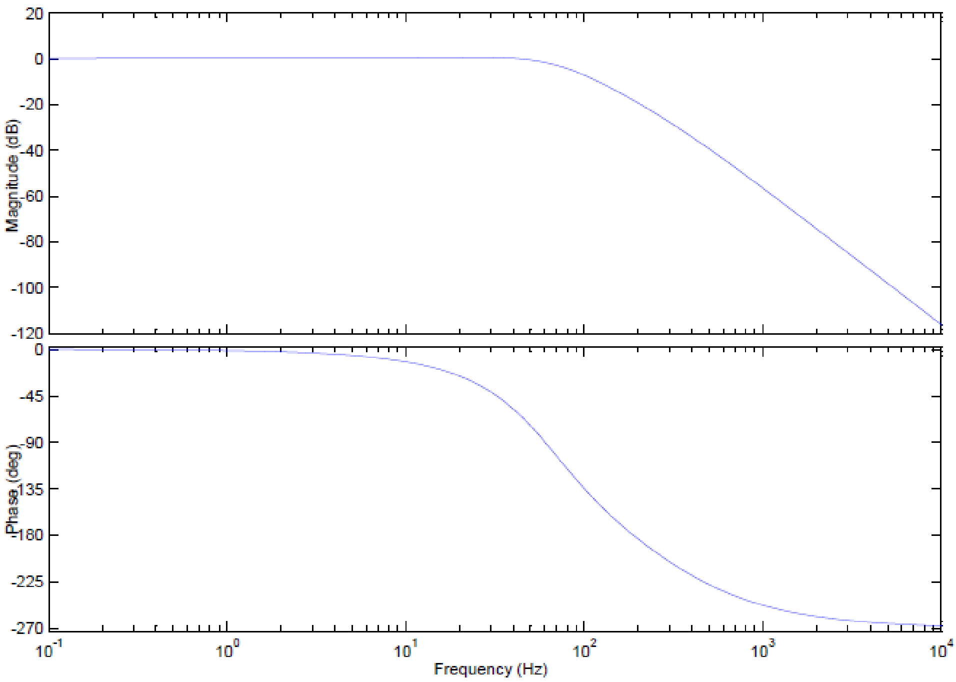

Figure 7. Bode diagram of the actuator

5. FINAL REMARKS

It was presented the digital prototyping of a magnetorheological knee for prostheses and exoskeletons. Digital prototyping environment was used for design and assembly the actuator’s parts. The prototype is driven by a Maxon EC 60 flat, brushless, 100 Watt DC motor with a Harmonic Drive CSD-17-2UH, 1:100, and a magnetorheological brake design to provide resistive torque.

The magnetic flux contour and the magnetic flux density in actuator’s brake was valuated and presented in Figure 3. The maximum flux density is such that no material saturation occurs. The density calculated on the fluid area is about 0.4337 T which satisfy the project’s design requirements, producing about 111 Nm of resistive torque.

It was also presented the actuator's performance. Figure 6 shows the step response of the actuator’s position and Figure 7 shows the frequency response of the magnitude and phase of the actuator’s position. The results show that the developed actuator is promising for the proposed applications.

Some improvements to the actuator itself will be needed for the next steps of the project, aiming to manufacture, assembly and testing. Future works will be in the construction of a physical prototype and testing its performance in a real time environment.

6. ACKNOWLEDGEMENTS

This research was partially funded by grants from the FAPES (Fundação de Amparo à Pesquisa do Espírito Santo) and UFES (Universidade Federal do Espirito Santo).

7. REFERENCES

Abreu, G. L. C. M. e Ribeiro, F. A., 2014, Modelagem matemática de um amortecedor com fluido magnetoreológico, CONEM 2014;

Carlson, J. D., Matthis, W. and Toscano, J. R., 2001, Smart prosthetics based on magnetorheological fluids, Proc. SPIE, 4332, 308–16;

Chen, J. Z., and Liao, W. H., 2010, Design, testing and control of a magnetorheological actuator for assistive knee braces, Smart Mater. Struct. ,19, 035029, (10pp);
Dong, S. F., Lu, K. Q., Sun, J. Q. and Rudolph, K., 2005, Rehabilitation device with variable resistance and intelligent control, Med. Eng. Phys., 27, 249–55;
Dong, S. F., Lu, K. Q., Sun, J. Q. and Rudolph, K., 2006, A prototype rehabilitation device with variable resistance and joint motion control, Med. Eng. Phys., 28, 348–55;
Filho, A. B., Andrade, R. M. e Matos, M. C., 2014, Digital Prototyping of a Series Elastic Actuator for Exoskeletons, CONEM 2014;
Garcia, E., Arevalo, J. C., MunOz, G., 2011, On the biomimetic design of agile-robot legs. Sensors, Basel, Switzerland, 11, 11305;
Grunwald, A., Olabi, A. G., 2008, Design of magnetorheological (MR) valve, Sens Actuators, A148, 211–223;
Gudmundsson, K. H., Jonsdottir, F. and Thorsteinsson, F., 2010, A geometrical optimization of a magneto-rheological rotary brake in a prosthetic knee, Smart Mater. Struct., 19, 035023;
Guo, H. T., and Liao, W. H., 2012, A novel multifunctional rotary actuator with magnetorheological fluid, Smart Mater. Struct., 21, 065012, (9pp);
Herr, H., Wilkenfeld, A., 2003, User-adaptive control of a magnetorheological prosthetic knee, Ind Rob., 30(1):42-55.;
Johansson, R., Robertsson, A., Nilsson, K., Brogårdh, T., Cederberg, P., Olsson, M., Olsson, T., Bolmsjö, G., 2004, "Sensor integration in task-level programming and industrial robotic task execution control", Industrial Robot: An International Journal, Vol. 31 Iss: 3, pp.284 – 296;
Kapti, A.O., Yucenur, M.S., 2006. Design and control of an active artificial knee joint. Mechanism and Machine Theory 41, 1477–1485.
Kavlicoglu, B. M., Gordaninejad, F., Evrensel, C., Fuchs, A. and Korol, G., 2006, A semi-active magnetorheological fluid limited slip differential clutch, Trans. ASME, J. Vib. Acoust., 128, 604–10;
Kawamoto, H. and Sankai, Y., 2002, Comfortable power assist control method for walking aid by HAL-3, Proc. IEEE Int. Conf. on Systems, Man and Cybernetics, 4, TP1B2;
Lauwerys, C., Swevers, J. and Sas, P., 2002, Linear control of car suspension using nonlinear actuator control, Proceedings do ISMA2002, Leuven-Bélgica;
Lima, A. S., 2011, Identificação Experimental de mm Sistema Magneto-Reológico, Tese de Doutorado, COPPE UFRJ.
Martinez-Villalpando. E. C., Her, H., 2009, Agonist-antagonist active knee prosthesis: A preliminary study in level-ground walking, J.Rehabilitation Res. Development, 46, 361-374;
Nguyen, Q. H. and Choi, S. B., 2010, Optimal design of an automotive magnetorheological brake considering geometric dimensions and zero-field friction heat, Smart Mater. Struct., 19, 115024;
Rainbow, J., 1948. The magnetic fluid clutch". AIEE Transactions, Vol. 67, pp. 1308–1315;
Riener, R., Rabuffetti, M., Frigo, C., 2002. Stair ascent and descent at different inclinations. Gait Posture 15, 32–44.
Robinson, W. (2000).“Design and analysis of series elasticity in closed-loop actuator force control”, Ph.D. Thesis, Massachusetts Institute of Technology.
Soyguder, S., Alli, H.. 2007, Design and prototype of a six-legged walking insect robot, Industrial Robot: An International Journal, 34, 5, 412-422;
Stutz, L. T., “Síntese e Análise de uma Suspensão Semi-Ativa Magneto Reológica Baseada na Abordagem de Controle com Estrutura Variável, Rio de Janeiro, 2005.
Sung, K. G., and Choi, S. B., 2008, Effect of an electromagnetically optimized magnetorheological damper on vehicle suspension control performance, Proc. Inst. Mech. Eng., 222, 2307–19;
Takashi, T., Sano, A., 2005, Fully Adaptive Vibration Control for Uncertain Structure Installed with MR Damper , American Control Conference, 2005. Proceedings of the 2005, 7, 4753 – 4759;
Takesue, N., Asaoka, H., Lin, J., Sakaguchi, M., Zhang, G. and Furusho, J., 2000, Development and experiments of actuator using MR fluid, Proc. 26th Annual Conf. IEEE Industrial Electronics Society, 3, 1838–43;
Wang, Z., 2011, Interactive virtual prototyping of a mechanical system considering the environment effect. Part 1: Modeling dynamics, Comptes Rendus Mécanique, 339, 9, 591-604;
Yang, G., 2001, Large-scale magnetorheological fluid damper for vibration mitigation: modeling, testing and control, PhD Dissertation University of Notre Dame, Indiana, USA.

8. RESPONSIBILITY NOTICE

The authors are the only responsible for the printed material included in this paper.